Catalysis Communications xxx (xxxx) xxx

Contents lists available at ScienceDirect

Catalysis Communications

journal homepage: www.elsevier.com/locate/catcom

Fast and efficient processes for oxidation and monitoring of polycyclic aromatic hydrocarbons in environmental matrices

Kelvin C. Araújo [a], Eryka T.D. Nóbrega [a], Ailton J. Moreira [b,*], Sherlan G. Lemos [c], Wallace D. Fragoso [c], Ernesto C. Pereira [a,*]

[a] Department of Chemistry - Federal University of São Carlos, São Carlos, SP, Brazil
[b] Institute of Chemistry, São Paulo State University (UNESP), Araraquara, SP, Brazil
[c] Department of Chemistry, Federal University of Paraíba, João Pessoa, PB, Brazil

ARTICLE INFO

Keywords:
Polyaromatic hydrocarbons
Emerging pollutants
Fluorescence excitation-emission matrix
PARAFAC
Advanced oxidation processes

ABSTRACT

This study proposes a new approach for the efficient photodegradation of polycyclic aromatic hydrocarbons (PAH) and derivatives. PAH removal was achieved in just a few minutes using a microwave photochemical reactor capable of producing a high concentration of $^{\bullet}OH$ (2.3 mmol L^{-1} h^{-1}). Fluorescence excitation-emission matrix (EEM) spectroscopy coupled to parallel factor analysis (PARAFAC) was used for quantifying two PAH and one alkylated PAH at low concentrations (μg L^{-1}). These results highlight the high potential of the photochemical degradation system coupled to EEM-PARAFAC as an alternative fast, inexpensive, and efficient approach for environmental remediation studies of PAH.

1. Introduction

Anthracene (ANT), naphthalene (NAP), and dibenzothiophene (DBT) are three organic compounds that belong to the class of polycyclic aromatic hydrocarbons (PAH) and alkylated PAH [1]. The incomplete combustion processes of organic materials, whether natural or anthropogenic, represent the primary sources of PAH in the environment. PAH are recognized for their persistence in various environmental matrices such as air, soil, sediment, and water [2]. Their existence raises environmental and health concerns, given that PAH is toxic to many organisms and can accumulate in the food chain [3,4]. ANT, NAP, and DBT are the main PAH and PAH-related substances observed in oil and other fossil fuel spills [5–9]. They have low molecular weight and high volatility, being pollutants with high environmental dispersion, causing an immediate impact on the quality of air, water, and human health. Given the potential risks associated with PAH, monitoring and mitigation efforts are crucial. Consequently, regulatory agencies like the United States Environmental Protection Agency (US EPA) and the European Community have classified these compounds as priority organic contaminants [10].

Hyphenated analytical techniques, such as gas chromatography–mass spectrometry (GC–MS), high-performance liquid chromatography (HPLC), and capillary electrophoresis (CE), are traditionally employed for the detection and quantification of PAH [11–13]. These methods offer distinct advantages, including accuracy and sensitivity. However, they also come with significant drawbacks, such as expensive equipment and high operating costs, which limit their widespread use. Additionally, using these instruments requires a high consumption of time and organic solvents, generally involving laborious separation and extraction methods under the supervision of highly skilled analysts.

PAH can also be quantified using luminescence techniques, like fluorescence spectroscopy [14,15]. This is possible due to their high quantum yield and relatively straightforward analysis. In the context of environmental analysis, fluorescence proves valuable for detecting and quantifying the presence of organic pollutants, heavy metals, and toxic chemicals [5,16–20], with sensitivity and selectivity, enabling the determination of trace amounts. Fluorescence methods do not require extensive sample treatment and can be carried out with much simpler instrumentation. When carried out as an emission-excitation matrix (EEM) three-dimensional analytical signal and combined with second-order calibration methods, like parallel factor analysis (PARAFAC), it is an outstanding strategy for the simultaneous identification and quantification of PAH in aqueous samples [21]. Furthermore, owing to the expeditious analysis of samples, often completed in <2 min, there is a notable reduction in analyte loss attributed to volatilization. This swift analytical process contributes to preserving sample integrity and

* Corresponding author.
E-mail addresses: ailton.moreira@unesp.br (A.J. Moreira), ernesto@ufscar.br (E.C. Pereira).

https://doi.org/10.1016/j.catcom.2023.106834
Received 8 October 2023; Received in revised form 12 December 2023; Accepted 25 December 2023
Available online 28 December 2023

enhances the reliability of results in the study context.

PAH can undergo degradation through various methods, including bioremediation, chemical degradation, thermal treatment, and photodegradation [22]. Analyzing the photochemical behavior of PAH is crucial for elucidating certain aspects of complex environmental systems. In this context, the study of the combined utilization of ultraviolet and microwave radiation has shown significant importance in advancing oxidation processes. This significance is mainly noticed when employing mercury discharge electrodeless lamps (Hg-MDEL), which enable high process efficiency [23,24]. Numerous studies have proved that microwave-powered electrodeless discharge lamp systems effectively generate hydroxyl radicals (•OH) [25,26]. In this regard, microwave irradiation has found widespread use in photocatalysis [27], substantially broadening its application scope to tackle diverse contaminants effectively. Notably, hazardous dyes [25,28,29] and pesticides [30] have been successfully decomposed through this approach. Within this experimental configuration, the microwave serves as the activator for the lamp, albeit with inherent inefficiencies in the lamp's operation. Of paramount significance is the observation that, despite their inherent efficiency, these systems are strategically employed in conjunction with semiconductors or oxidizing agents. This strategic synergy is implemented to enhance the operational processes' overall efficiency systematically.

Thus, it allows us to consider the importance of evaluating its application in PAH degradation. To our knowledge, this is the first study of the Hg-MDEL application in degrading PAH. From a different standpoint, our study deliberately omitted the use of semiconductors or oxidizing agents, concentrating solely on assessing the lamp's influence on the degradation of emerging contaminants. This approach allows for a focused exploration of the lamp's effects within the context of contaminant degradation, excluding potential confounding variables introduced by semiconductor or oxidizing agent interactions. Therefore, the presented work aimed to evaluate the use of Hg-MDEL in the photodegradation of anthracene, naphthalene, and dibenzothiophene via a developed analytical method based on the association between EEM and PARAFAC. The study introduces novel approaches, representing a pioneering effort in evaluating the efficacy of this technique for environmental remediation. This uniqueness contributes to advancing scientific understanding and highlights the relevance of this research in the broader landscape of environmental pollutant analysis and remediation.

2. Experimental

2.1. Photochemical degradation system

For the photodegradation studies, a photochemical reactor consisting of a microwave discharge electrodeless mercury lamp (Hg-MDEL, UMEX, Dresden, Germany), with a functional capacity of 10 mL [23,31] and a microwave equipment (2450 MHz, 11.5 A, 1300 W, Electrolux, Manaus, Amazonas, Brazil) was used. The degradation process involved adding 10 mL of the mixture to the reactor. The reactor was operated at a microwave power of 900 W for times ranging from 0.083 to 1 min, and at the end of each degradation time, the samples were subjected to chemical analysis. The initial concentrations of the PAH in the mixture were 17.2 ± 0.2 μg L^{-1} for ANT (Sigma Aldrich, 99%), 16.4 ± 0.7 μg L^{-1} for NAP (Sigma Aldrich, 99%), and 183.8 ± 2.7 μg L^{-1} for DBT (Sigma Aldrich, 98%). Photodegradation assays of PAH in the presence of a scavenger for hydroxyl radicals [dimethyl sulfoxide (DMSO, Sigma Aldrich, 99%)] were also performed. In this assay, a volume of 100 μL of DMSO was added for each 10 mL of the solution to be degraded.

Probe assays for •OH using coumarin (COU, Sigma Aldrich, 99%) were carried out in the photochemical system. A volume of 10 mL of a 1.5 mg/L COU solution was added to the Hg-MDEL lamp and irradiated under the same conditions as the PAH degradation assays. In the presence of •OH, COU is converted to 7-hydroxycoumarin (7HC, umbelliferone), which has an emission peak centered on 460 nm when excited at 330 nm [32]. A calibration curve based on the 7HC analytical standard was constructed by applying solutions with a concentration of 1 to 20 μg L^{-1}. The concentration of •OH produced was calculated as described in the literature [33].

2.2. Spectra acquisition and data processing

The excitation-emission matrices (EEM) for PAH and 7HC were acquired using a Shimadzu spectrofluorometer (RF5301pc, Tokyo, Japan), with an aperture of 5 nm for the excitation and emission slits for ANT, NAP, or DBT, and 5 nm for the excitation slit and 3 nm for the emission slit for 7HC. The scanning conditions and maximum peaks for excitation and emission are described in Table 1. A 3.5 mL cuvette with a 1 cm optical path was used.

The subtraction of ultrapure water EEM from sample EEM was carried out to remove Raman scattering. PARAFAC was employed to decompose sample spectra and separate each mixture component. The quantification of these components was performed using a pseudo-univariate curve. The algorithm was implemented using the N-Way toolbox [34] through the graphical interface of MVC2 in MATLAB [35]. The number of components was estimated based on the value of the residual standard deviation (s_{fit}) [5,15,36]. The limits of detection (LOD) and quantification (LOQ) were estimated from the limit of blank as presented in [37].

A high-performance liquid chromatograph with a fluorescence detector (Shimadzu, model DGU-20 A5, Prominence, RF 20 A detector) was also used to analyze the degraded PAH samples using the following chromatographic conditions: flow rate: 1 mL/min, elution gradient: (FA) Formic Acid 0.1% (*v*/v) / (ACN) Acetonitrile, 0 min: 50%FA/50%ACN, 0-5 min: 30%FA/70%ACN, 5-10 min: 10%FA/90%ACN, 10–10.5 min: 50%FA/50%ACN, 10.5-11 min: 50%FA/50%ACN. Column temperature: 30 °C. Detection: $\lambda_{exc.} = 250$ nm and $\lambda_{em.} = 405$ nm for ANT, $\lambda_{exc.} = 275$ nm and $\lambda_{em.} = 340$ nm for NAP and $\lambda_{exc.} = 285$ nm and $\lambda_{em.} = 335$ nm for DBT. Phenomenex Luna column, C18, 5 μm, 100 Å, 150 × 4.6 mm. Under these conditions, a calibration curve was constructed for each PAH.

3. Results and discussion

3.1. Identification and quantification of PAH

Figure 1 shows the EEM spectra of the aqueous standards of ANT (Fig. 1a), NAP (Fig. 1b), and DBT (Fig. 1c) prepared in water collected from natural sources.

By applying PARAFAC to the EEM data collected from the mixture of PAH, four components were identified and recovered for calibration curve construction. Three of these components correspond to ANT, NAP, and DBT, as identified in Fig. 2.

The fourth component could be attributed to organic matter naturally present in surface waters, as reported in the literature [38]. Table 2 shows the figures of merit of the method.

The efficiency of the methodology for quantifying ANT, NAP, and DBT in environmental matrices was confirmed, even in the presence of potential interferences such as natural organic matter (Fig. 2). The LOD and LOQ achieved were compatible with many studies on the degradation of PAH in environmental matrices and for environmental

Table 1
Experimental and instrumental information about the compounds studied.

Compound	λ_{exc} (nm) range	λ_{em} (nm) range	λ_{exc} $(nm)_{max}$	λ_{em} $(nm)_{max}$
ANT	230–300	310–450	250	382/406/426
NAP			275	324/334
DBT			284	336
7HC	265–350	380–480	327	456

Note: The analysis time for PAH was 2 min, and for 7HC, it was 2.5 min.

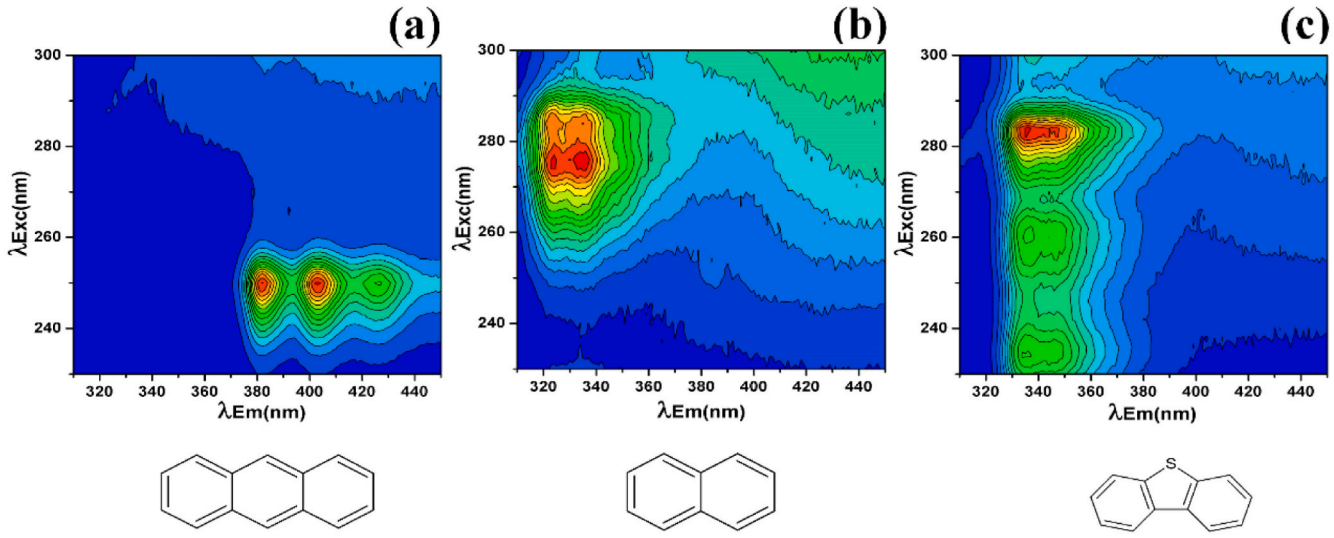

Fig. 1. EEM spectra of ANT (a), NAP (b), and DBT (c) standard in a surface water sample.

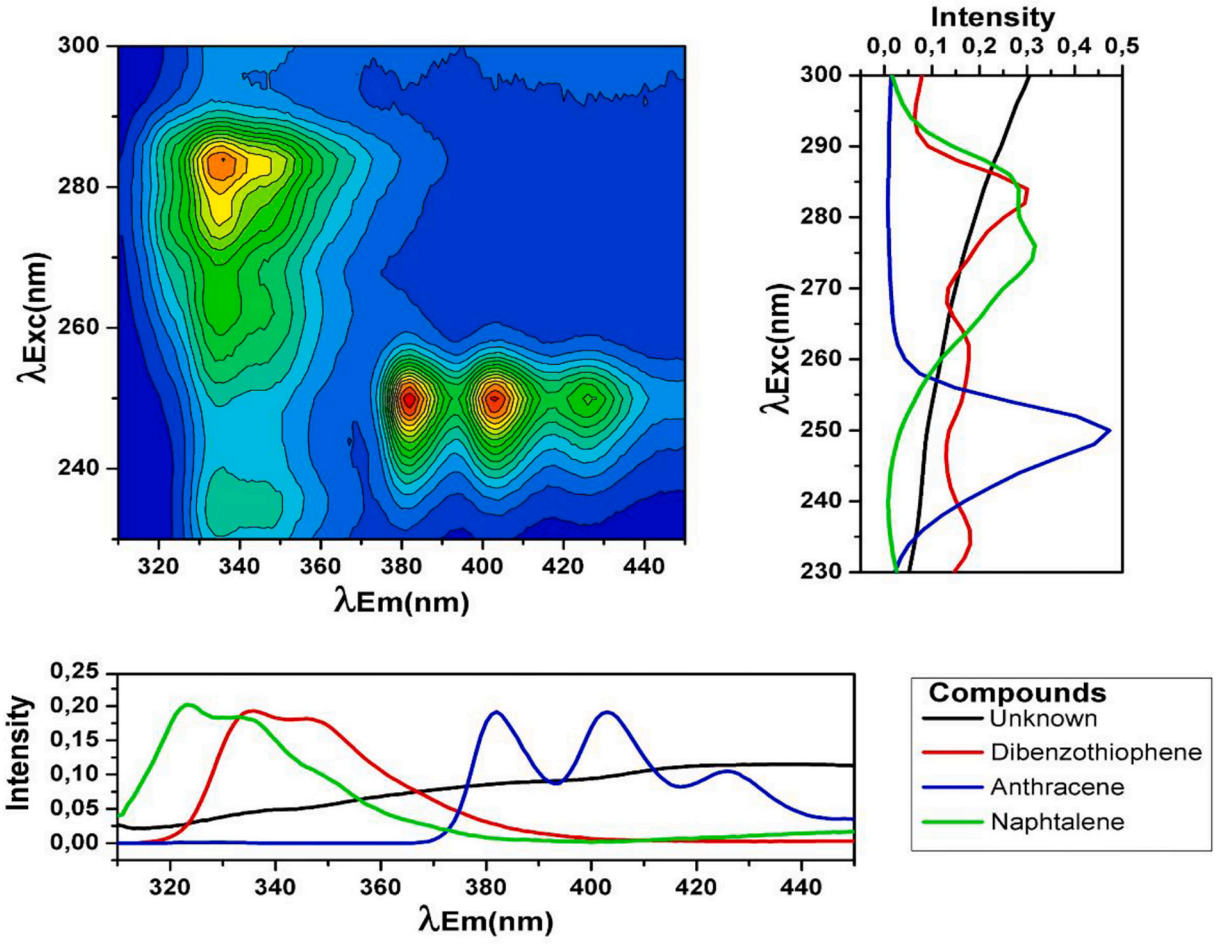

Fig. 2. EEM spectra of an ANT, NAP, and DBT mixture prepared in a surface water matrix.

monitoring purposes, highlighting the applicability of the method [39–41]. Other advantages include the high analytical throughput and the greener and lower cost characteristics compared to the conventional methods based on chromatography [42,43]. The results for HPLC-RF showed greater sensitivity; however, the analysis time required for each sample was 11 min with the generation of organic residues from

Table 2
Figures of merit of the EEM-PARAFAC and HPLC RF methods for quantifying PAH.

Compound	Linear range (μg L^{-1})	Linear coefficient (R^2)	LOD / LOQ (μg L^{-1})
EEM - PARAFAC			
ANT	0.5–20	0.998	0.43 / 1.43
NAP	5–100	0.998	2.68 / 8.91
DBT	10–250	0.996	1.46 / 4.86
HPLC-RF			
ANT	0.1–50	0.999	0.002 / 0.006
NAP	0.1–50	0.996	0.01 / 0.03
DBT	1–500	0.999	0.41 / 1.36

the mobile phase. Spectrofluorometers are widely available in chemical laboratories and have lower cost than HPLC-RF. Thus, its use to monitor PAH in advanced oxidation studies could be an excellent alternative. Considering the excellent results of the quantification methodology, it was applied in analyzing a mixture of PAH degraded by a photocatalytic process unreported in the literature to treat such environmental pollutants.

3.2. Photochemistry degradation of PAH

In the photodegradation assays, a photochemical system that has already shown high efficiency for the degradation of pharmaceuticals and pesticides was used [23,44] to evaluate its potential for the degradation of PAH. Fig. 3 shows the changes in EEM spectra of the samples at 0, 0.25, and 1.0 min, corresponding to the mixture before and after two periods of photochemical degradation (Fig. 3a-c).

After processing the EEM data using PARAFAC, the ratios of the final/initial concentrations (C/Co) of the PAH over the degradation time of the pure solutions of each PAH (Fig. 3d), the mixture (Fig. 3e), and the mixture containing DMSO (Fig. 3f) were obtained. ANT removal showed high efficiency, and its degradation curve for the pure solution, the mixture, and the mixture with DMSO confirm that ANT is wholly degraded in 0.083 min. The literature shows that one of the mechanisms for the photochemical degradation of ANT is the breaking of the pi bonds in the central ring. This causes a discontinuity in the electronic conjugation of the aromatic structure and consequent loss of the fluorescent property [45]. In continuing the mechanism, species such as anthrone and anthraquinone can be produced by hydroxyl radical (•OH) attack. Still, as these by-products are not fluorescent, no signal is observed [45,46]. The maximum degradation of NAP in the mixture or individual solution was 88% and 79% in 1 min, respectively (Fig. 3d-e). The more excellent removal of naphthalene in the mixture may be associated with forming other reactive species arising from the degradation of ANT or DIB. This hypothesis is also reinforced by the 100% degradation of NAP when DMSO is added to the mixture (Fig. 3f). The DBT degradation also shows high efficiency in a short irradiation time. In just 0.5 min, 98% of DBT is degraded in the individual solution or mixture, achieving 98% removal in 0.42 min when DMSO is added.

For comparison purposes, HPLC-RF and EEM-PARAFAC analyses were carried out for the raw and degraded mixture at 0.25, 0.5, and 1.0 min. Fig. 4 shows the recovered chromatograms of ANT (Fig. 4a), NAP (Fig. 4b), and DBT (Fig. 4c) for the raw mixture and the degraded in 0.5 min. The calibration curves obtained to quantify the analytes by HPLC-RF (Fig. 4d) were applied, and the removal of PAH calculated by the EEM-PARAFAC and HPLC-RF methods were compared in Fig. 4e. The errors of the samples that achieved >95% PAH removal were not added because the concentrations obtained were below the LOQ of the method applied. The average removal values obtained for the HPLC-RF method and EEM-PARAFAC are comparable, confirming that EEM-PARAFAC is an excellent alternative for monitoring PAH in advanced oxidation studies.

As the photochemical system has already been characterized in previous studies and a high efficiency in •OH forming has been confirmed [23], it is possible to infer that the degradation of PAH could

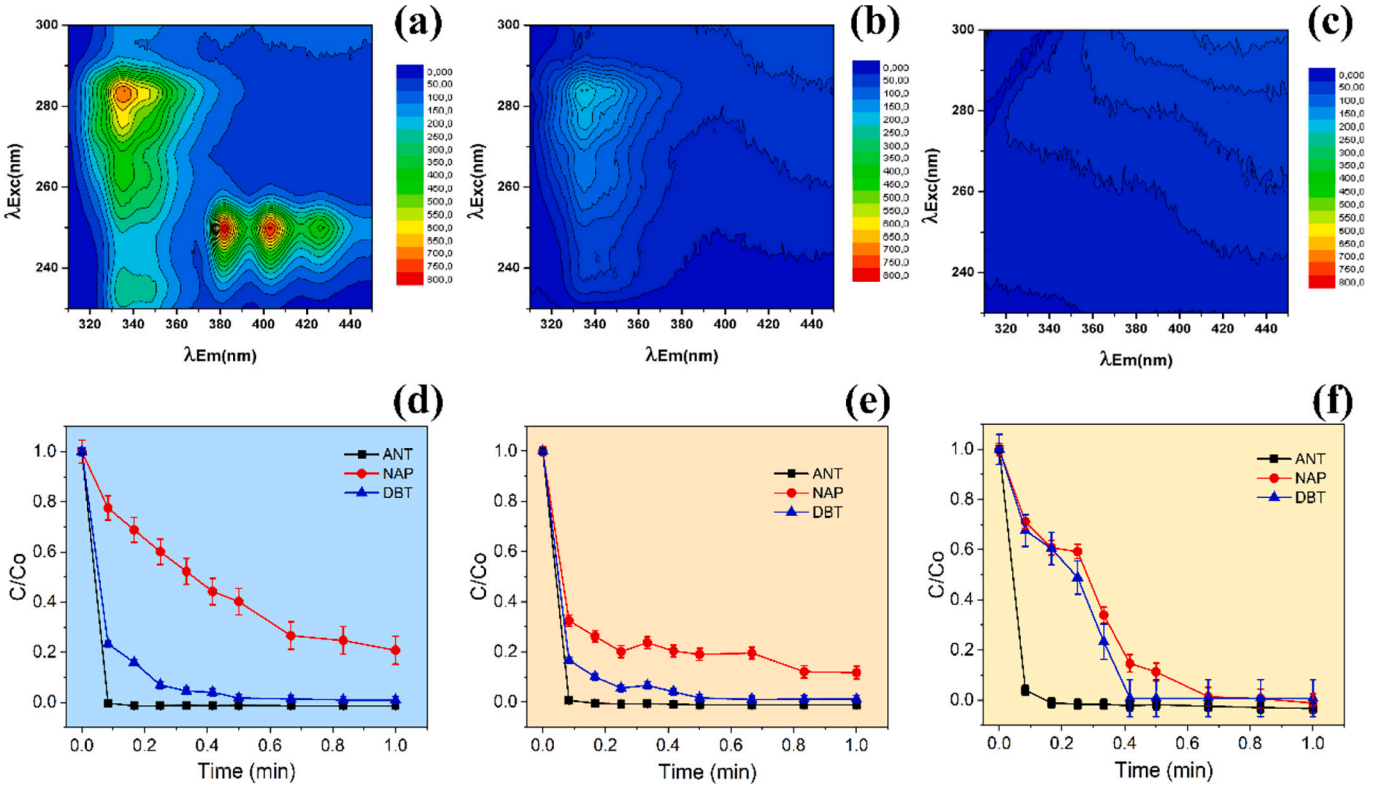

Fig. 3. EEM spectrum recovered from the original sample (a) and degraded at 0.25 min (b) and 1.0 min (c). Degradation curves of PAH alone (d), in the mixture (e), and the mixture containing DMSO (f).

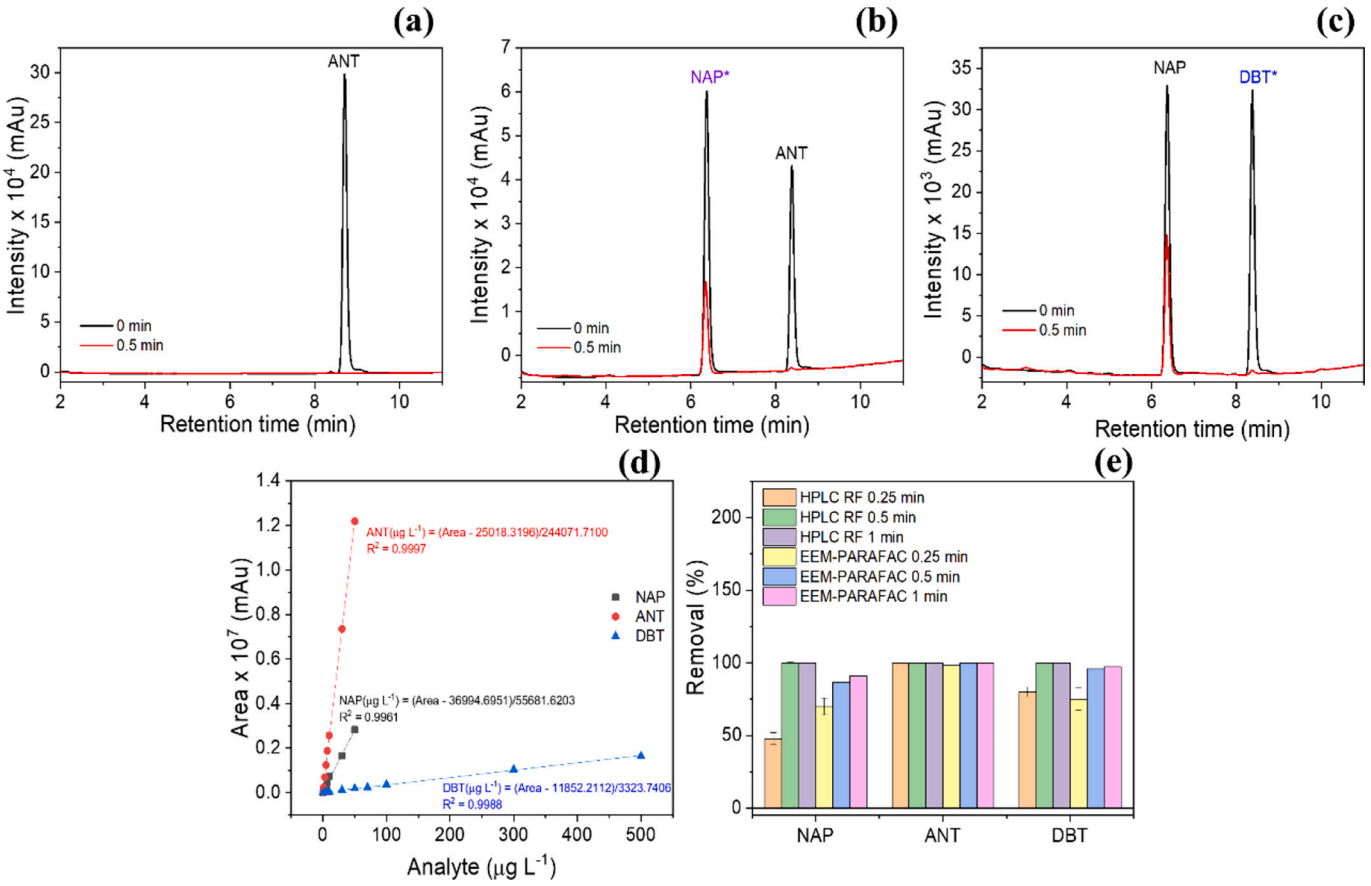

Fig. 4. Chromatograms of the PAH mixture under the analytical conditions for the quantification of ANT (a), NAP (b), DBT (c), and calibration curve (d). Comparative PAH removal data after the photolytic process comparing the concentrations calculated by the EEM-PARAFAC and HPLC-RF methods (e).

occur through •OH attack. The literature shows that the reaction of DMSO with •OH promotes the formation of methyl radicals, which may be the reactive species responsible for reacting with NAP and DBT to improve their removal. As these methyl radicals can also be produced by the photolysis of ANT, NAP, or DIB, the better degradation in the mixture is also justified [47]. To prove this hypothesis, •OH probe assays were carried out on the reaction with coumarin. Fig. 5a shows the EEM data and the profile recovered by PARAFAC used to quantify 7HC. It should be noted that 7HC is the oxidation product of coumarin by •OH identified by the heat region in the EEM spectrum with $\lambda_{exc.} = 330$ nm and $\lambda_{em.} = 460$ nm.

The figures of merit were LOD = 0.247 μg L^{-1}, LOQ = 0.748 μg L^{-1} and $R^2 = 0.999$. In addition to 7HC, EEM-PARAFAC recovered two unknown components (C2, C3) (Fig. 5a), which may be additional COU oxidation by-products. However, the emission intensities of these compounds are negligible compared to 7HC under the conditions of analysis applied. Fig. 5b shows the change in concentration of 7HC at the different irradiation times, reaching its maximum at 0.083 min and a significant drop after this time. These results are compatible with our previous study, which proved that 7HC is oxidized when •OH is produced in excess [23], with the consequent formation of 4-hydroxycoumarin (4HC), which was not quantified in this study. Fig. 5 c-d shows that the 7HC fluorescence signal disappears entirely in just 0.25 min, confirming the oxidation of 7HC. Using the equation proposed by Nagarajan et al. [48], the concentration of •OH produced in just 0.083 min was 3.2 μmol L^{-1} or 2.3 mmol L^{-1} h^{-1}, which is well above the amount of •OH produced in other photochemical systems reported in the literature [47,48]. Therefore, the high removal efficiency of PAH in a short time is due to the effective production of •OH from the photolysis of water promoted by the Hg-MDEL lamp activated at 900 W.

As the degradation of PAH in the mixture was greater and did not allow data to be collected at degradation times, the pseudo-first-order kinetic constants (k = min^{-1}) of the individual solutions calculated for NAP and DBT were k = 1.51 min^{-1} / R^2 = 0.975 and k = 6.04 min^{-1} / R^2 = 0.960, respectively. To ANT, the k value was not obtained due to total degradation in <0.1 min. As one can see, no changes in the ANT degradation profile were observed, which allows us to state that its degradation mechanism is mediated by photolysis and not by hydroxyl radical oxidation under the experimental conditions applied. However, the degradations of NAP and DBT were inhibited compared to that observed in a DMSO-free mixture. Thus, NAP and DBT oxidation occurs mainly via •OH action, which explains the high removal values in just 1 min.

To highlight the competitiveness of the analytical and degradation methods investigated in this study, we compared our results with others reported in the literature under approximate application conditions. In addition to achieving competitive LOD / LOQ, the method used in this study allows analytical data to be obtained 96% faster compared to more sophisticated techniques. Another positive feature is that no residue is produced from the chemical analysis, which is carried out in a much cheaper and easier-to-operate instrument compared to chromatographic techniques. For the degradation process using the system proposed in this study, the comparative data (Table 3) confirm that even without adding catalysts or other oxidizing agents, the removal of PAH is much higher than the data found in the literature [49].

4. Conclusions

A fast, efficient, and cost-effective methodology has been successfully achieved to identify and quantify a mixture of ANT, NAP, and DBT

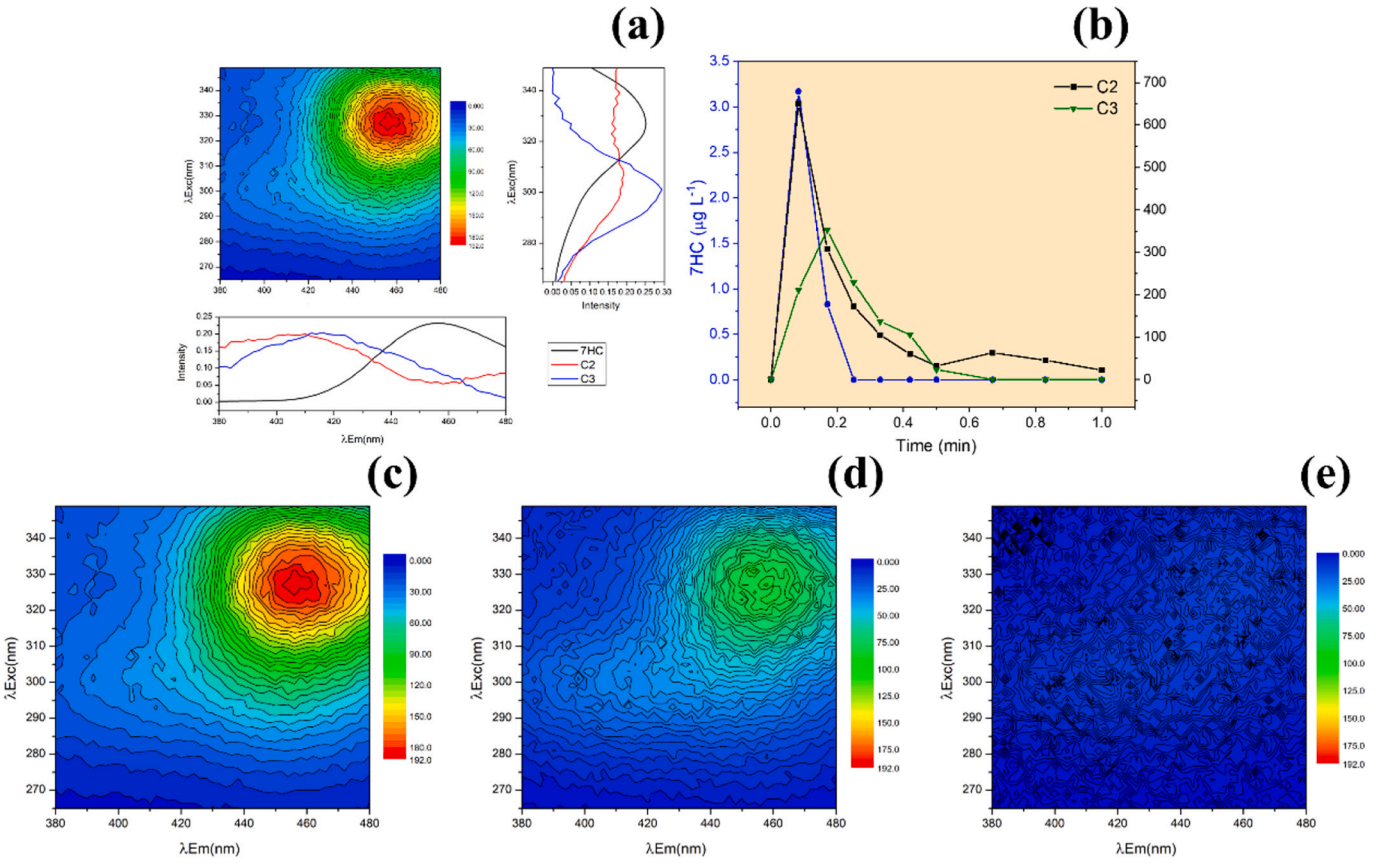

Fig. 5. EEM spectrum of COU and profiles recovered by PARAFAC (a). Evolution of 7HC, C2, and C3 during coumarin photolysis up to 1 min (b). EEM spectra obtained during the irradiation of COU at 0.25 min (c), 0.5 min (d), or 1 min (e).

Table 3
Comparative data on ANT, NAP, and DBT quantification methods and degradation processes.

Quantification de PAH				
Analytical method	LOQ / LOD ($\mu g\ L^{-1}$)	Instrumental analysis time (min)	Chemical residue from the analysis	Reference
EEM-PARAFAC	8.91 / 2.68 (NAP) 1.43 / 0.43 (ANT) 4.86 / 1.46 (DBT)	2	no residue	This is work
GC-TOF-MS*	- / 3.4 (NAP) - / 0.52 (ANT) - / 0.17 (DBT)	30	dichloromethane, hexane.	[50]
LC-DAD*	5.0 / 1.5 (ANT)	45	acetonitrile	[12]
LC-UV*	0.25 / 0.083 (NAP)	12	acetonitrile	[51]
LC-PDA*	4200 / 1390 (DBT)	25	acetonitrile	[52]

Degradation of PAH under UV light				
Degradation process	Initial concentration ($\mu g\ L^{-1}$)/volume (mL)	Kinetic constant ($k = min^{-1}$)/R^2	Total removal (%)/Time (min)	Reference
Photolysis Hg-MDEL	17.2 / 10 (ANT) 183.8 / 10 (DBT) 16.4 / 10 (NAP)	1.51 / 0.975 6.04 / 0.960 -	100 / 0.083 (ANT) 99 / 0.5 (DBT) 88 / 0.83 (NAP)	This is work
TiO_2	5000 / -	0.008 / 0.998	94 / 180 (NAP)	[53]
Photolysis UV	500 / 2000	2.03 / 0.951	99 / 15 (ANT)	[54]
UV-H_2O_2	12 / 2000	–	100 / 2 (ANT)	[55]
$LaZn_{0.5}Ti_{0.5}O_3$	300.000/100	0.09 / 0.97	100 / 30 (DBT)	[56]

* Requires extraction processes and sample preparation before analysis.

in natural waters using EEM. The low LOD and LOQ achieved are compatible with many studies reported in the literature, and the method's accessibility is highlighted. A photochemical system activated by microwave radiation could degrade a mixture of ANT, NAP, and DBT at environmentally relevant concentrations in less than one minute. The high efficiency was attributed to the effective production of $^{\bullet}OH$ (2.3 mmol L^{-1} h^{-1}) from the photolysis of water, which ensured the degradation of PAH in just 1 min. The $^{\bullet}OH$ was quantified by a method

that has also been little explored and used the EEM-PARAFAC to identify and quantify 7HC used in the quantitative calculations of •OH. Based on the excellent results, we hope that the use of fluorescence coupled with second-order calibration can help the community in the analysis and monitoring of organic contaminants, identification, and quantification of •OH. The high degradation efficiency for the photochemical system incentivizes new reactor configurations to be studied to scale up the application process for environmental remediation. In addition to being fast and efficient, the photodegradation system does not require using catalytic compounds such as semiconductors, peroxide, persulphate, and others to achieve the excellent degradation of emerging contaminants.

Author contributions

Kelvin A. Costa: Writing - original draft, Methodology. **Eryka T.D. Nobrega:** Methodology, Writing, review & editing. **Ailton J. Moreira:** Methodology, Writing, review & editing. **Sherlan G. Lemos:** Methodology, Validation, Writing, review & editing. **Wallace D. Fragoso:** Methodology, Validation, Writing, review & editing. **Ernesto C. Pereira:** Resources, Supervision, Writing, review & editing.

Ernesto C. Pereira: Writing, review & editing.

CRediT authorship contribution statement

Kelvin C. Araújo: Methodology, Writing – original draft, Writing – review & editing. **Eryka T.D. Nóbrega:** Investigation, Methodology, Writing – review & editing. **Ailton J. Moreira:** Investigation, Methodology, Writing – review & editing. **Sherlan G. Lemos:** Methodology, Validation, Writing – review & editing. **Wallace D. Fragoso:** Methodology, Validation, Writing – review & editing. **Ernesto C. Pereira:** Resources, Supervision, Writing – review & editing.

Declaration of Competing Interest

There are no conflicts of interest to declare.

Data availability

Data will be made available on request.

Acknowledgments

This work was financially supported by Coordenação de Aperfeiçoamento de Pessoal de Nível Superior (CAPES) - Finance Code 001, Fundação de Amparo à Pesquisa do Estado de São Paulo (grants: 2013/07296-2, 2022/06219-3, 2022/05254-0), Conselho Nacional de Desenvolvimento Científico e Tecnológico (CNPq) grants: 383432/2023-5, DTI-A, and Shell. J. A.

References

[1] A. Mojiri, J.L. Zhou, A. Ohashi, N. Ozaki, T. Kindaichi, Comprehensive review of polycyclic aromatic hydrocarbons in water sources, their effects and treatments, Sci. Total Environ. 696 (2019) 133971, https://doi.org/10.1016/j.scitotenv.2019.133971.

[2] A.L. Bolden, J.R. Rochester, K. Schultz, C.F. Kwiatkowski, Polycyclic aromatic hydrocarbons and female reproductive health: a scoping review, Reprod. Toxicol. 73 (2017) 61–74, https://doi.org/10.1016/j.reprotox.2017.07.012.

[3] T.M. Gutiérrez-Valencia, M.P. García de Llasera, On-line MSPD-SPE-HPLC/FLD analysis of polycyclic aromatic hydrocarbons in bovine tissues, Food Chem. 223 (2017) 82–88, https://doi.org/10.1016/j.foodchem.2016.11.099.

[4] N. Akvan, G. Azimi, H. Parastar, Chemometric assisted determination of 16 PAHs in water samples by ultrasonic assisted emulsification microextraction followed by fast high-performance liquid chromatography with diode array detector, Microchem. J. 150 (2019) 104056, https://doi.org/10.1016/j.microc.2019.104056.

[5] K.C. Araújo, M.C. Barreto, A.S. Siqueira, A.C.P. Freitas, L.G. Oliveira, M.E.P. A. Bastos, M.E.P. Rocha, L.A. Silva, W.D. Fragoso, Oil spill in northeastern Brazil: application of fluorescence spectroscopy and PARAFAC in the analysis of oil-related compounds, Chemosphere. 267 (2021), https://doi.org/10.1016/j.chemosphere.2020.129154.

[6] L.G. Oliveira, K.C. Araújo, M.C. Barreto, M.E.P.A. Bastos, S.G. Lemos, W. D. Fragoso, Applications of chemometrics in oil spill studies, Microchem. J. 166 (2021) 106216, https://doi.org/10.1016/j.microc.2021.106216.

[7] W.G. Mendoza, D.D. Riemer, R.G. Zika, Application of fluorescence and PARAFAC to assess vertical distribution of subsurface hydrocarbons and dispersant during the Deepwater horizon oil spill, Environ Sci Process Impacts 15 (2013) 1017, https://doi.org/10.1039/c3em30816b.

[8] A Review on Polycyclic Aromatic Hydrocarbons_ Source, Environmental Impact, Effect on Human Health and Remediation.pdf, (n.d.).

[9] S.M. Mudge, Reassessment of the hydrocarbons in Prince Williams sound and the Gulf of Alaska: identifying the source using partial least-squares, Fuel Energy Abstr. 44 (2003) 73, https://doi.org/10.1016/S0140-6701(03)90527-3.

[10] USEPA, Drinking Water Standards and Health Advisories, (n.d.). http://www.epa.gov/OST/orderpubs.html.

[11] P. Avino, I. Notardonato, L. Perugini, M.V. Russo, New protocol based on high-volume sampling followed by DLLME-GC-IT/MS for determining PAHs at ultra-trace levels in surface water samples, Microchem. J. 133 (2017) 251–257, https://doi.org/10.1016/j.microc.2017.03.052.

[12] F.C. Turazzi, L. Morés, E. Carasek, J. Merib, G.M. de Oliveira Barra, A rapid and environmentally friendly analytical method based on conductive polymer as extraction phase for disposable pipette extraction for the determination of hormones and polycyclic aromatic hydrocarbons in river water samples using high-performance l, J. Environ. Chem. Eng. 7 (2019) 103156, https://doi.org/10.1016/j.jece.2019.103156.

[13] L. Ferey, N. Delaunay, D.N. Rutledge, A. Huertas, Y. Raoul, P. Gareil, J. Vial, I. Rivals, An experimental design based strategy to optimize a capillary electrophoresis method for the separation of 19 polycyclic aromatic hydrocarbons, Anal. Chim. Acta 820 (2014) 195–204, https://doi.org/10.1016/j.aca.2014.02.040.

[14] J.S. Miller, Determination of polycyclic aromatic hydrocarbons by spectrofluorimetry, Anal. Chim. Acta 388 (1999) 27–34, https://doi.org/10.1016/S0003-2670(99)00067-7.

[15] A.S. Siqueira, L.F. Almeida, W.D. Fragoso, Determination of anthracene, phenanthrene, and fluorene in tap water and sediment samples by fluorescence spectroscopy on nylon membranes and second-order calibration, Talanta. 253 (2023) 124002, https://doi.org/10.1016/j.talanta.2022.124002.

[16] S.O. Tümay, M.H. Irani-nezhad, A. Khataee, Development of dipodal fluorescence sensor of iron for real samples based on pyrene modified anthracene, Spectrochim. Acta - Part A Mol. Biomol. Spectrosc. 261 (2021), https://doi.org/10.1016/j.saa.2021.120017.

[17] X. Niu, Y. Zhong, R. Chen, F. Wang, Y. Liu, D. Luo, A "turn-on" fluorescence sensor for Pb2+ detection based on graphene quantum dots and gold nanoparticles, Sensors Actuators B Chem. 255 (2018) 1577–1581, https://doi.org/10.1016/j.snb.2017.08.167.

[18] S.O. Tümay, M.H. Irani-Nezhad, A. Khataee, Multi-anthracene containing fluorescent probe for spectrofluorimetric iron determination in environmental water samples, Spectrochim. Acta - Part A Mol. Biomol. Spectrosc. 248 (2021), https://doi.org/10.1016/j.saa.2020.119250.

[19] R. Ye, H. Fang, Y.-Z. Zheng, N. Li, Y. Wang, X. Tao, Fabrication of CoTiO 3 /g-C 3 N 4 hybrid Photocatalysts with enhanced H 2 evolution: Z-scheme photocatalytic mechanism insight, ACS Appl. Mater. Interfaces 8 (2016) 13879–13889, https://doi.org/10.1021/acsami.6b01850.

[20] S.O. Tümay, V. Şanko, E. Demirbas, A. Şenocak, Fluorescence determination of trace level of cadmium with pyrene modified nanocrystalline cellulose in food and soil samples, Food Chem. Toxicol. 146 (2020), https://doi.org/10.1016/j.fct.2020.111847.

[21] S.A. Bortolato, J.A. Arancibia, G.M. Escandar, A novel application of nylon membranes to the luminescent determination of benzo[a]pyrene at ultra trace levels in water samples, Anal. Chim. Acta 613 (2008) 218–227, https://doi.org/10.1016/j.aca.2008.03.004.

[22] A.K. Haritash, C.P. Kaushik, Biodegradation aspects of polycyclic aromatic hydrocarbons (PAHs): a review, J. Hazard. Mater. 169 (2009) 1–15, https://doi.org/10.1016/j.jhazmat.2009.03.137.

[23] A.J. Moreira, A.C. Borges, B.B. De Souza, L.R. Barbosa, V.R. De Mendonça, C. D. Freschi, G.P.G. Freschi, Microwave discharge electrodeless mercury lamp (hg-MDEL): an energetic, mechanistic and kinetic approach to the degradation of Prozac, J. Environ. Chem. Eng. 7 (2019), https://doi.org/10.1016/j.jece.2019.102916.

[24] S. Horikoshi, M. Kajitani, S. Sato, N. Serpone, A novel environmental risk-free microwave discharge electrodeless lamp (MDEL) in advanced oxidation processes, J. Photochem. Photobiol. A Chem. 189 (2007) 355–363, https://doi.org/10.1016/j.jphotochem.2007.02.027.

[25] Y. Ju, J. Fang, X. Liu, Z. Xu, X. Ren, C. Sun, S. Yang, Q. Ren, Y. Ding, K. Yu, L. Wang, Z. Wei, Photodegradation of crystal violet in TiO2 suspensions using UV-vis irradiation from two microwave-powered electrodeless discharge lamps (EDL-2): products, mechanism and feasibility, J. Hazard. Mater. 185 (2011) 1489–1498, https://doi.org/10.1016/j.jhazmat.2010.10.074.

[26] L. Xue, C. Zhao, J. Liu, N. Zhong, J. Zhang, K. Huang, Microwave electrodeless UV light source combine ozone generation with photocatalytic simultaneous degradation of norfloxacin, Chem. Eng. Process. Process Intensif. 186 (2023), https://doi.org/10.1016/j.cep.2023.109325.

[27] S. Horikoshi, H. Hidaka, N. Serpone, Environmental remediation by an integrated microwave/UV-illumination method. 1. Microwave-assisted degradation of

rhodamine-B dye in aqueous TiO2 dispersions, Environ. Sci. Technol. 36 (2002) 1357–1366, https://doi.org/10.1021/es010941r.
[28] C. Ferrari, H. Chen, R. Lavezza, C. Santinelli, I. Longo, E. Bramanti, Photodegradation of rhodamine B using the microwave/UV/H2O 2: effect of temperature, Int. J. Photoenergy. 2013 (2013), https://doi.org/10.1155/2013/854857.
[29] Microwave-Assisted-Rapid-Photocatalytic-Degradation-of-Malachite-Green-in-tio2-Suspensions-Mechanism-and.pdf, (n.d.).
[30] G. Zhanqi, Y. Shaogui, T. Na, S. Cheng, Microwave assisted rapid and complete degradation of atrazine using TiO2 nanotube photocatalyst suspensions, J. Hazard. Mater. 145 (2007) 424–430, https://doi.org/10.1016/j.jhazmat.2006.11.042.
[31] A.J. Moreira, A.C. Borges, L.F.C. Gouvea, T.C.O. MacLeod, G.P.G. Freschi, The process of atrazine degradation, its mechanism, and the formation of metabolites using UV and UV/MW photolysis, J. Photochem. Photobiol. A Chem. 347 (2017) 160–167, https://doi.org/10.1016/j.jphotochem.2017.07.022.
[32] A.J. Moreira, J.O.D. Malafatti, T.R. Giraldi, E.C. Paris, E.C. Pereira, V.R. de Mendonça, V.R. Mastelaro, G.P.G. Freschi, Prozac® photodegradation mediated by Mn-doped TiO<inf>2</inf> nanoparticles: evaluation of by-products and mechanisms proposal, J. Environ. Chem. Eng. 8 (2020), https://doi.org/10.1016/j.jece.2020.104543.
[33] Comparative Assessment of Visible Light and UV Active Photocatalysts by Hydroxyl Radical Quantification.pdf, (n.d.).
[34] R. Bro, PARAFAC., Tutorial and applications, Chemom. Intell. Lab. Syst. 38 (1997) 149–171, https://doi.org/10.1016/S0169-7439(97)00032-4.
[35] A.C. Olivieri, H.-L. Wu, R.-Q. Yu, MVC2: a MATLAB graphical interface toolbox for second-order multivariate calibration, Chemom. Intell. Lab. Syst. 96 (2009) 246–251, https://doi.org/10.1016/j.chemolab.2009.02.005.
[36] A.C. Olivieri, G.M. Escandar, Parallel factor analysis, in: Pract. Three-w. Calibration, Elsevier, 2014, pp. 65–92, https://doi.org/10.1016/B978-0-12-410408-2.00005-3.
[37] M.C. Barreto, R.G. Braga, S.G. Lemos, W.D. Fragoso, Determination of melamine in milk by fluorescence spectroscopy and second-order calibration, Food Chem. 364 (2021) 130407, https://doi.org/10.1016/j.foodchem.2021.130407.
[38] S. Dong, Y. Gong, Z. Zeng, S. Chen, J. Ye, Z. Wang, D.D. Dionysiou, Dissolved organic matter promotes photocatalytic degradation of refractory organic pollutants in water by forming hydrogen bonding with photocatalyst, Water Res. 242 (2023) 120297, https://doi.org/10.1016/j.watres.2023.120297.
[39] M. Sayed, B. Ren, A.M. Ali, A. Al-Anazi, M.N. Nadagouda, A.A. Ismail, D. D. Dionysiou, Solar light induced photocatalytic activation of peroxymonosulfate by ultra-thin Ti3+ self-doped Fe2O3/TiO2 nanoflakes for the degradation of naphthalene, Appl. Catal. B Environ. 315 (2022) 121532, https://doi.org/10.1016/j.apcatb.2022.121532.
[40] Z. Cai, F. Yang, Y. Song, Y. Liu, W. Liu, Q. Wang, X. Sun, Semiconducting mineral induced photochemical conversion of PAHs in aquatic environment: mechanism study and fate prediction, Sci. Total Environ. 860 (2023) 160382, https://doi.org/10.1016/j.scitotenv.2022.160382.
[41] N.S. Hassan, A.A. Jalil, C.N.C. Hitam, M.H. Sawal, M.N.S. Rahim, I. Hussain, N.W. C. Jusoh, R. Saravanan, D. Prasetyoko, Enhanced photooxidative desulphurization of dibenzothiophene over fibrous silica tantalum: influence of metal-disturbance electronic band structure, Int. J. Hydrog. Energy 48 (2023) 6575–6585, https://doi.org/10.1016/j.ijhydene.2022.02.008.
[42] X. Guo, F. Chen, W. Zhang, Pollution level, source, and health risk assessment of PAHs in food products and environmental media in Nantong, China: a pilot case, J. Food Compos. Anal. 123 (2023) 105624, https://doi.org/10.1016/j.jfca.2023.105624.
[43] P. Ghosh, S. Mukherji, Fate, detection technologies and toxicity of heterocyclic PAHs in the aquatic and soil environments, Sci. Total Environ. 892 (2023) 164499, https://doi.org/10.1016/j.scitotenv.2023.164499.
[44] J.O.D. Malafatti, A.J. Moreira, C.R. Sciena, T.E.M. Silva, G.P.G. Freschi, E. C. Pereira, E.C. Paris, Prozac® removal promoted by HAP:Nb2O5nanoparticles system: by-products, mechanism, and cytotoxicity assessment, J. Environ. Chem. Eng. 9 (2021), https://doi.org/10.1016/j.jece.2020.104820.
[45] X. Li, H. Zhao, B. Qu, Y. Tian, Photoformation of environmentally persistent free radicals on particulate organic matter in aqueous solution: role of anthracene and formation mechanism, Chemosphere. 291 (2022) 132815, https://doi.org/10.1016/j.chemosphere.2021.132815.
[46] M. Baruah, S.L. Ezung, S. Sharma, U. Bora Sinha, D. Sinha, Synthesis and characterization of Ni-doped TiO2 activated carbon nanocomposite for the photocatalytic degradation of anthracene, Inorg. Chem. Commun. 144 (2022) 109905, https://doi.org/10.1016/j.inoche.2022.109905.
[47] M.G. Steiner, C.F. Babbs, Quantitation of the hydroxyl radical by reaction with dimethyl sulfoxide, Arch. Biochem. Biophys. 278 (1990) 478–481, https://doi.org/10.1016/0003-9861(90)90288-A.
[48] S. Nagarajan, N.C. Skillen, F. Fina, G. Zhang, C. Randorn, L.A. Lawton, J.T. S. Irvine, P.K.J. Robertson, Comparative assessment of visible light and UV active photocatalysts by hydroxyl radical quantification, J. Photochem. Photobiol. A Chem. 334 (2017) 13–19, https://doi.org/10.1016/j.jphotochem.2016.10.034.
[49] M.P. Rayaroth, M. Marchel, G. Boczkaj, Advanced oxidation processes for the removal of mono and polycyclic aromatic hydrocarbons – a review, Sci. Total Environ. 857 (2023) 159043, https://doi.org/10.1016/j.scitotenv.2022.159043.
[50] W.B. Studabaker, K.J. Puckett, K.E. Percy, M.S. Landis, Determination of polycyclic aromatic hydrocarbons, dibenzothiophene, and alkylated homologs in the lichen Hypogymnia physodes by gas chromatography using single quadrupole mass spectrometry and time-of-flight mass spectrometry, J. Chromatogr. A 1492 (2017) 106–116, https://doi.org/10.1016/j.chroma.2017.02.051.
[51] F.N. Serenjeh, P. Hashemi, A.R. Ghiasvand, F. Rasolzadeh, N. Heydari, A. Badiei, Cooling assisted headspace microextraction by packed sorbent coupled to HPLC for the determination of volatile polycyclic aromatic hydrocarbons in soil, Anal. Chim. Acta 1125 (2020) 128–134, https://doi.org/10.1016/j.aca.2020.05.067.
[52] P. Ghosh, S. Mukherji, Desorption kinetics of soil sorbed carbazole, fluorene, and dibenzothiophene by P. Aeruginosa RS1 from single and multicomponent systems and elucidation of their interaction effects, Biochem. Eng. J. 180 (2022) 108367, https://doi.org/10.1016/j.bej.2022.108367.
[53] C.N. Rani, S. Karthikeyan, Synergic effects on degradation of a mixture of polycyclic aromatic hydrocarbons in a UV slurry photocatalytic membrane reactor and its cost estimation, Chem. Eng. Process. Process Intensif. 159 (2021) 108179, https://doi.org/10.1016/j.cep.2020.108179.
[54] A. Rubio-Clemente, E. Chica, G.A. Peñuela, Photolysis of a mixture of anthracene and benzo[a]pyrene at ultra-trace levels in natural water with disinfection purposes, J. Environ. Sci. 92 (2020) 79–94, https://doi.org/10.1016/j.jes.2020.02.002.
[55] A. Rubio-Clemente, E. Chica, G.A. Peñuela, Photovoltaic array for powering advanced oxidation processes: sizing, application and investment costs for the degradation of a mixture of anthracene and benzo[a]pyrene in natural water by the UV/H2O2 system, J. Environ. Chem. Eng. 6 (2018) 2751–2761, https://doi.org/10.1016/j.jece.2018.03.046.
[56] M.R. Madkour, S. Abdel-Azim, A.M. Ashmawy, E.M. Elnaggar, D. Aman, Perovskite nanomaterials with exceptional photocatalytic properties for oxidative desulfurization of dibenzothiophene, J. Ind. Eng. Chem. (2023), https://doi.org/10.1016/j.jiec.2023.07.007.